Exp Brain Res (2005) 165: 273–282
DOI 10.1007/s00221-005-2298-6

RESEARCH ARTICLE

**Pavlos Gourtzelidis · Charidimos Tzagarakis
Scott M. Lewis · David A. Crowe · Edward Auerbach
Trenton A. Jerde · Kâmil Uğurbil
Apostolos P. Georgopoulos**

Mental maze solving: directional fMRI tuning and population coding in the superior parietal lobule

Received: 10 September 2004 / Accepted: 1 February 2005 / Published online: 7 June 2005

Abstract The superior parietal lobule (SPL) of six human subjects was imaged at 4 T during mental traversing of a directed maze path. Here we demonstrate the orderly involvement of the SPL in this function, as follows. Forty-two percent of the voxels were tuned with respect to the direction of the maze path. This suggests a coherent tuning of local neuronal populations contributing to the change of the single-voxel BOLD signal. Preferred directions ranged throughout the directional continuum of 360°. Voxels with similar preferred directions tended to cluster together: on average there were seven same-direction clusters per slice, with an average cluster membership of five voxels/cluster and an average nearest-neighbor same-direction intercluster distance of 13.1 mm. On the other hand, the average nearest-neighbor intercluster distance between a given direction and all other directions was 3.1 mm. This suggests a patchy arrangement such that patches of directionally tuned voxels, containing voxels with different preferred directions, alternate with patches of non-tuned voxels. Finally, the population vector predicted accurately the direction of the maze path (with an error of 12.7°), and provided good estimates (with an error of 29°) when calculated within parts of the SPL. Altogether, these findings document a new, orderly functional organization of the SPL with respect to mental tracing.

Keywords Superior parietal lobule · fMRI
Directional tuning · Spatial cognition · Mental tracing

P. Gourtzelidis · C. Tzagarakis · S. M. Lewis · D. A. Crowe
T. A. Jerde · A. P. Georgopoulos (✉)
Brain Sciences Center, Veterans Affairs Medical Center,
One Veterans Drive, Minneapolis, MN 55417, USA
E-mail: omega@umn.edu
Tel.: +612-725-2282
Fax: +612-725-2291

P. Gourtzelidis · C. Tzagarakis · D. A. Crowe
A. P. Georgopoulos
Department of Neuroscience,
University of Minnesota Medical School,
Minneapolis, MN 55455, USA

S. M. Lewis · A. P. Georgopoulos
Department of Neurology,
University of Minnesota Medical School,
Minneapolis, MN 55455, USA

S. M. Lewis · T. A. Jerde · K. Uğurbil · A. P. Georgopoulos
Graduate Program in Neuroscience, University of Minnesota,
Minneapolis, MN 55455, USA

E. Auerbach · K. Uğurbil
Center for Magnetic Resonance Research,
University of Minnesota, Minneapolis, MN 55455, USA

E. Auerbach · K. Uğurbil
Department of Radiology, University of Minnesota Medical
School, Minneapolis, MN 55455, USA

T. A. Jerde · A. P. Georgopoulos
Center for Cognitive Sciences, University of Minnesota,
Minneapolis, MN 55455, USA

A. P. Georgopoulos
Department of Psychiatry, University of Minnesota Medical
School, Minneapolis, MN 55455, USA

Introduction

The parietal cortex is involved in various visuospatial and visuoconstructive functions, including mental rotation (Cohen et al. 1996; Tagaris et al. 1996, 1997, 1998; Alivisatos and Petrides 1997; Harris et al. 2000; Bestmann et al. 2002; Harris and Miniussi 2003), route following (Angelini et al. 1992), copying (Benton 1967), and object construction (Benton 1967), as evidenced by the kinds of deficits of people with parietal damage (Benton 1967; Angelini et al. 1992) and by the results of studies of parietal function in healthy people using functional neuroimaging methods (Cohen et al. 1996; Tagaris et al. 1996, 1997, 1998; Alivisatos and Petrides 1997; Harris et al. 2000) or transcranial magnetic stimulation (Bestmann et al. 2002; Harris and Miniussi

2003). However, little is known about the functional representation of visuospatial information in the parietal cortex. In this work, we investigated the representation of the direction of mental tracing of a spatial path in the superior parietal lobule (SPL).

Materials and methods

Subjects

Six healthy, right-handed human subjects [two women and four men, age (mean ± SD) 24.8 ± 4.9 years] participated in these experiments as paid volunteers. The study protocol was approved by the University of Minnesota Institutional Review Board and informed consent was obtained before the study.

Stimuli and tasks

The maze was composed of white lines on a black background and subtended ~5°×5° of visual angle. It contained a central start box and a straight path extending outwards from the start box in one of eight radial directions (Fig. 1). This path either extended to the perimeter of the maze or terminated one path width from the perimeter of the maze. Maze fragments in the remaining interior area of the maze were randomly generated. Because there was a gap in the perimeter of the maze for an exit path, two more such gaps (for a total of three) were added at random locations in the perimeter to ensure that the subjects could not solve the maze on the basis of the presence of a gap. For no-exit mazes, three gaps were randomly added to the maze perimeter to keep the number of gaps constant for exit and no-exit mazes. Stimuli were presented as blocks of trials of 48 s total duration.

There were two kinds of task, in blocks, namely a control task followed by a maze task (Fig. 1). In both tasks, stimuli lasted for 300 ms and were presented every 2 s, for a total of 24 trials per block. This short presentation was intended to minimize the period of visual stimulation and potential eye movements. In the control task, only the grid stimulus was presented, and the subjects pushed a left or right button at random. In the maze task, maze stimuli were shown and the subjects had to indicate the exit status (present or absent) of the maze by pushing the right or left button, respectively. Mazes with different main path directions were presented in a randomized block design (one direction per block), always preceded by the control task block. Each maze block comprised equal proportions of exit and no-exit mazes in a random order. Subjects were instructed to fixate a central spot throughout the experiment. We have shown previously (Chafee et al. 2002) that this task can be performed with eyes fixated. The eyes of the subjects were monitored using a video camera; no obvious eye movements were observed. Subjects performed at 93%, or better, correct for both exit and no-exit mazes.

Imaging methods

A 4 T whole-body system (90-cm bore) with head gradients and a homogeneous radio-frequency coil [Oxford (Oxford, UK)/Varian (Palo Alto, CA, USA)/Siemens (Erlangen, Germany)] was used. A head-support system with foam pads was used to minimize head movements during the experiment. Multi-slice axial, sagittal, and coronal anatomic images (T1-weighted) were obtained

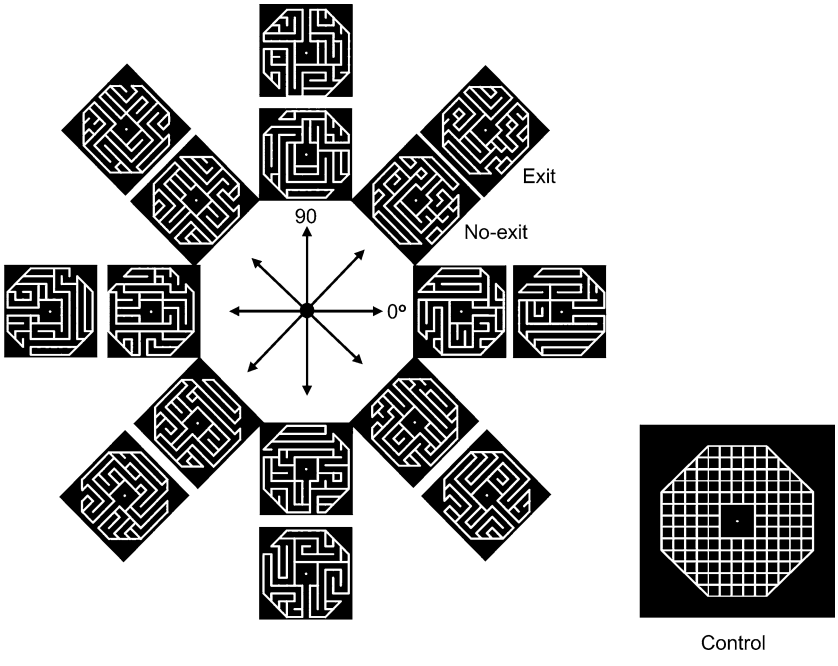

Fig. 1 Representative mazes. The directions of the maze path are shown in the middle. The control grid is also shown

from the whole brain using an inversion-recovery (IR) TurboFLASH sequence (TI = 1.2 s, TE = 4.4 ms, TR = 8.8 ms, matrix = 128×128, FOV = 20 cm×20 cm, in-plane resolution: 1.56 mm×1.56 mm, slice thickness = 5 mm, NEX = 4). These images were used for anatomic localization of the activated voxels and to select the appropriate volume for functional imaging. The sagittal images were used to select the appropriate oblique plane for imaging of the SPL (Fig. 2). This plane was selected using the superior extension of the parietal–occipital sulcus and the marginal ramus of the cingulate sulcus as landmarks. We then obtained five contiguous oblique slices using the IR TurboFLASH sequence (slice thickness = 3 mm) to confirm an imaging volume centered on the surface of the SPL, bilaterally, and extending inferiorly with the following borders: anterior–precentral gyrus, posterior–lateral extension of the parietal–occipital sulcus, lateral–inferior parietal lobule. We then obtained T2* weighted functional images of the same volume using four segment EPI (TE = 25 ms, 4 segments w/navigator, matrix = 128×128, FOV = 20×20 cm, slice thickness = 3 mm, five oblique slices). The TR was 750 ms and the time between volumes was 750 ms×4 segments = 3 s. Five images (not used for any analyses) were acquired for stabilization of longitudinal magnetization, followed by 32 volumes for each control + maze task block (16 for control and 16 for task sub-blocks) resulting in a task-related acquisition time of 96 s. The acquisition was repeated for each of the eight maze directions. The fMRI analysis package Stimulate (version 5.8.1, Center for Magnetic Resonance Research, University of Minnesota Medical School, Minneapolis, MN, USA) was used to process the fMRI images. Images were screened for motion artifacts by measuring variation in the center of mass of functional images over the entire time course. This measurement was performed separately for the X, Y, and Z coordinates. Subject motion was further assessed by forming a cine loop of the images. Both measurements were performed using the fMRI analysis program Stimulate, above.

Fig. 2 Location of the five imaging planes in the SPL

Data analysis

General

The SPL was defined anteriorly by the postcentral sulcus, posteriorly by the lateral extension on the parietal–occipital sulcus, laterally by the medial edge of the intraparietal sulcus, and medially by the interhemispheric fissure. All analyses were performed on individual voxels located within the SPL. The BMDP/Dynamic statistical package (BMDP Statistical Software, Los Angeles, CA, USA; 1992), the SPSS 10.1 statistical package for Windows (SPSS, Chicago, IL, USA; 2000), and ad-hoc programs were used to implement the various analyses. Data were detrended using a sliding regression algorithm to take out low-frequency noise (Marchini and Ripley 2000); an example is shown in Fig. 3.

For each voxel-task and control block, time series of 16 data points were available; of these, the first two were rejected to enable stabilization of the hemodynamic response. The average BOLD value of the corresponding control block was subtracted from each of the 14 values of the task block and the data subjected to a repeated measures analysis of variance (ANOVA) (Snedecor and Cochran 1989) in which the sequential image number was a within-factor and the maze-path direction was a between-factor. This analysis assessed whether there was a statistically significant effect of maze-path direction ($P < 0.05$). Next, a multiple linear regression was performed on those voxels which showed a significant directional effect in the ANOVA, using the preprocessed BOLD data as the dependent variable and the x–y components of the maze-path direction as the independent variables. A statistically significant effect ($P < 0.05$) indicated the presence of directional tuning, and the preferred direction was calculated (Georgopoulos et al. 1982). For some analyses, the preferred directions were binned in eight bins using the four cardinal directions and the main diagonals as centers of the bins and a bin width of ± 22.5°.

Previous work in 4 T has indicated that the BOLD responses are likely to be multiplicative in nature (Georgopoulos et al. 2001; Lewis et al. 2002, 2003). This finding suggests that the data might need to be log-transformed to revert to additivity. We repeated all the analyses above (and those below) after log-transforming the data. We found that the results were almost identical, most probably because the effects observed were strong and robust, so the increase in sensitivity offered by the logarithmic transformation was not a major factor. However, had the results been marginal, it is likely this transformation would have made a substantial difference.

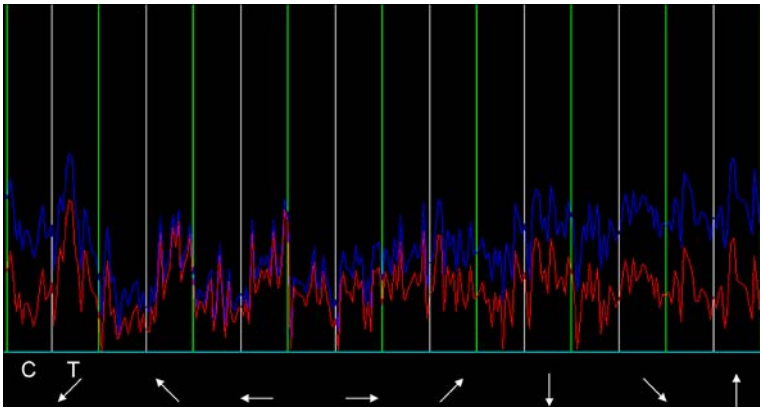

Fig. 3 Example of a raw (*blue*) and detrended (*red*) single-voxel time course. The ordinate is strength of the BOLD signal (arbitrary units). Intervals separated by green vertical lines denote a control + task (maze) block; control (*C*) and task (maze) (*T*) sub-blocks are separated by a *light grey line*. Each sub-block consists of 16 images. The direction of the maze path is indicated by *arrows*. Notice the removal of linear trends at the beginning and near the end of the time course without affecting the fine within-block variation in the BOLD signal

Permutation analysis

In the analyses above, many tests (ANOVAs and regressions) were carried out, because each was performed on data from each voxel. It is, therefore, possible that the percentage of directionally tuned voxels thus identified might be inflated. We evaluated this problem by performing a permutation analysis, as follows. For each voxel, the complete data set included 256 detrended time-course BOLD values (8 maze-path directions×16 images per block×2 tasks). Let k be the total number of voxels in a subject-hemisphere-slice; this yields a total of 256 k BOLD values. These values were randomly permuted and all the statistical analyses were performed in a manner identical with that used for the original, non-permuted data. This was done for each subject-hemisphere-slice, and the overall percentage (across all subjects) of directionally tuned voxels (i.e. with a statistically significant effect on both the ANOVA and the regression) was calculated in 1 million permutations. We wanted to determine the number of times that the percentage of directionally tuned voxels observed in the original data (42%) was obtained (or exceeded) in the permuted data.

Clustering analysis

Initial inspection of plots of the binned preferred directions in hemisphere-slices revealed there was substantial partial overlap, although voxels with specific preferred directions tended to cluster. To evaluate this quantitatively, we first excluded spatial outliers based on the following criterion. In a given hemisphere-slice, we calculated the pairwise distances between all directionally tuned voxels with preferred direction in a certain bin; we excluded from the clustering analysis voxels which were >7.8125 mm away from all other voxels. This value corresponds to five voxels (each voxel was 1.5625 mm square in-plane). Although this criterion is, at face value, somewhat arbitrary, it was effective at excluding outliers, as judged by visual inspection of directional voxel plots. Next, we quantified the clustering by performing an overlapping non-hierarchical clustering analysis (Corter 1996) using a K-means clustering algorithm (Aldenderfer and Blashfield 1984). This analysis partitions iteratively a set of cases (in our application, directionally tuned voxels in a hemisphere-slice). At the end of the run each case belongs to the cluster whose center is closest in Euclidean distance to the case. (The center of a cluster is defined as the mean of the cases in the cluster.) Data were analyzed on a hemisphere-slice basis (per subject and per binned direction), as follows. First, data points were plotted to obtain an initial estimate of the number of clusters. This number was specified in the KM-Means BMDP program and data points standardized according to the within-cluster covariance. The program yielded voxel membership shown in plots of the clusters identified. In addition, cluster statistics were given, namely:

1 the number of voxels in a cluster, their x–y means and standard deviations, and

2 an ANOVA table showing the mean squares of between-cluster and within-cluster x–y variation, and the corresponding values of the F-statistic and its significance values.

The final number of clusters was arrived at by inspecting the cluster plot, to ensure there was no obvious cluster overlap, and requiring a significance level of the between/within F-statistic of $P<0.001$ in the x- or y-dimension. Clusters with two or more voxels were included in further analyses.

A major quantitative objective of this analysis was to derive estimates of the distances between nearest neighbor clusters of the same direction. For that purpose, we calculated the average minimum distance between same-direction clusters for each direction and each hemisphere-slice. The same measure was also computed between a given direction and all other directions.

Population vector analysis

The population vector was calculated from ensembles of directionally tuned voxels, as follows.

1 For each directionally tuned voxel, i, the average BOLD intensity during the control task, c_i, was calculated.
2 Similarly, the average BOLD intensity m_{ij} was calculated for each direction j of the maze task ($n=8$ directions).
3 For a given direction, each voxel made a vectorial contribution in the direction of the voxel's preferred direction and of magnitude w_{ij} equal to the change in BOLD intensity from the control task: $w_{ij}=m_{ij}-c_i$.
4 The population vector P for the jth direction is $\mathbf{P}_j = \sum_1^k w_{ij}\mathbf{V}_i$, where V_i is the preferred direction of the ith voxel.

Results

Directional tuning

Of 41,530 total voxels contained within the SPL ($n=6$ subjects), 34,227 (82.4%) showed a significant directional effect in an ANOVA; of those, 17,589/34,227 (51.4%) were directionally tuned. An example of a directionally tuned voxel is shown in Figs. 4 and 5.

With respect to the whole voxel population, 17,589/41,530 = 42.4% voxels were directionally tuned. In the permutation analysis (see "Materials and methods"), not even once was this percentage achieved or exceeded in 1 million permutations. Therefore, the probability that the observed value is because of chance is $P<10^{-6}$. With respect to the two hemispheres, the results were very similar: the percentage of voxels with a significant ANOVA was 16,334/19,259 (84.8%) and 17,893/22,271 (80.3%), for the left and right hemispheres, respectively, and that with significant directional tuning was 8,446/16,334 (51.7%) and 9,143/17,893 (51.1%).

To determine the general form of the tuning curve, all tuning curves were standardized with respect to their range, aligned to their maximum and averaged across voxels. The result was a population directional tuning curve, shown in Fig. 6. It can be seen that the directional tuning was prominent, because the activation dropped to approximately one-half of the maximum at $\pm 45°$ away from it. Finally, preferred maze-path directions ranged throughout the directional continuum. Their circular distributions, for the left and right hemispheres, are shown in Fig. 7 as circular histograms (Mardia 1972). For both hemispheres, there was an overall downward bias and a slight contralateral bias with respect to upward directions.

Clustering

Similar preferred directions tended to cluster. In a nearest neighbor analysis (Figs. 8 and 9), we calculated the minimum distance between each voxel and the voxel with a reference preferred direction in the range $d \pm 22.5°$. Color-coded maps of these minimum distances are shown in Figs. 8 and 9 for two ranges of d centered on opposite directions. It can be seen that:

1 voxels with similar preferred directions tended to cluster,
2 preferred directions were represented repeatedly, and
3 voxels with approximately opposite preferred directions tended to occupy complementary spaces in the SPL.

In a different analysis (K-means clustering), we identified clusters consisting of voxels with the same (binned) preferred direction. The spatial distribution of voxel clusters in two opposite directions in a slice is shown in Fig. 10. Typically, multiple clusters were identified in a given slice (Fig. 11). On average ($\pm$SEM) there were 7 ± 0.2 same-direction clusters per slice containing 5.45 ± 0.06 voxels per cluster ($N=2{,}884$). The average minimum distance between the x and y centers of same-direction (nearest neighbor) clusters per hemisphere-slice was 13.1 ± 0.4 mm ($N=441$). Finally, the minimum distance between the x and y center of a certain directional cluster and those of all other

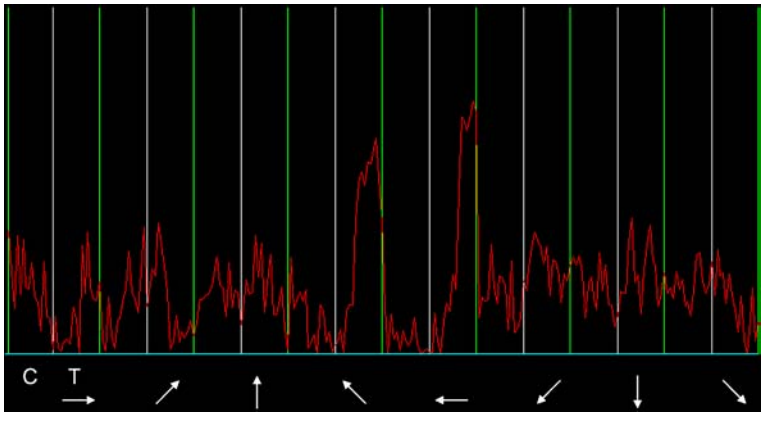

Fig. 4 Example of a detrended, directionally tuned, single-voxel time course. Conventions as in Fig. 3. maze-path directions have been re-ordered in an orderly sequence, from 0° (3 o'clock) counterclockwise. Notice the clear activation at 135 and 180°

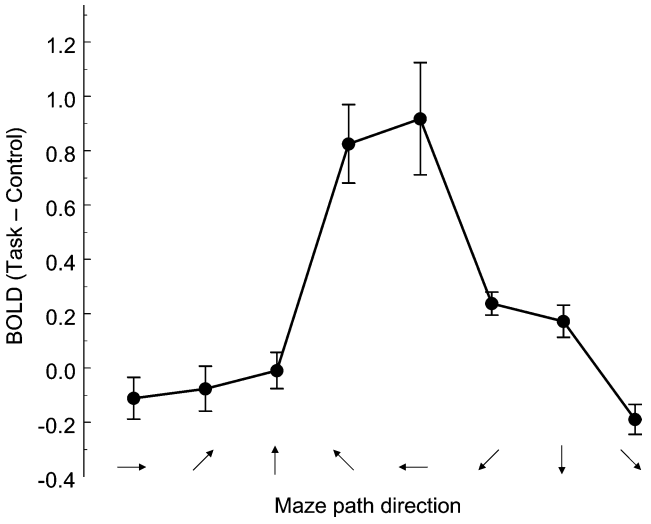

Fig. 5 Directional tuning curve of the data shown in Fig. 4 for a single voxel. Data points are mean ± SEM, $N = 14$ images (see text) from a single voxel

directions was 3.1 ± 0.06 mm ($N = 1594$). All of these measurements and relations were very similar in the two hemispheres, as were the relative location of clusters.

Population vector

The neuronal population vector, calculated from the whole ensemble of 17,589 directionally tuned voxels, predicted very well the direction of the maze path (Fig. 12). The average absolute angular error in predicting the maze-path direction was 12.72 ± 3.41°. The correlation coefficient in the linear fit shown in Fig. 12 was $r = 0.99$ ($P < 0.0001$); the slope did not differ significantly from 1, and the intercept did not differ significantly from zero. These results show that the population vector is an excellent and unbiased estimator of the maze-path direction. Remarkably, the population vector was found to be an excellent predictor of maze-path direction even when calculated from small, spatially adjacent, directionally tuned voxels (Fig. 13). The data illustrated in Fig. 13 indicate that ~150 voxels are sufficient to reach a plateau at an absolute angular error of ~31°, which is ~18° higher than that calculated from the whole ensemble of 17,589 directionally tuned voxels (12.7°). This finding emphasizes the substantial partial overlap of the various preferred directions.

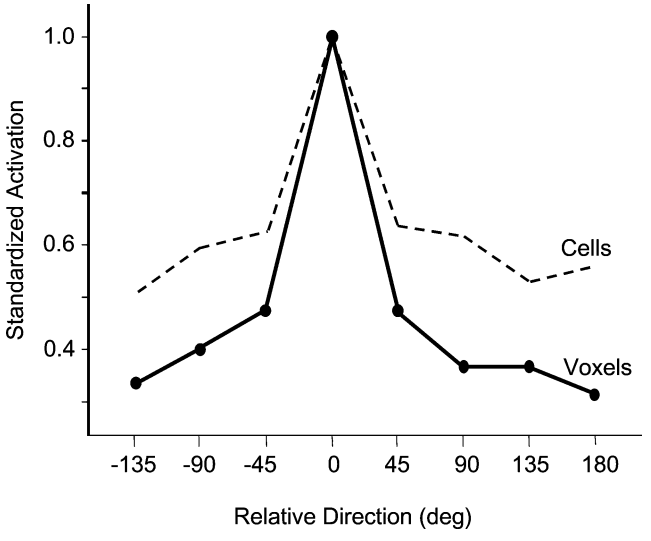

Fig. 6 Standardized population tuning curve (see text) for voxels and cells. The cell tuning curve is from Fig. 6 in Crowe et al. (2004)

Discussion

These results demonstrate, for the first time, the directional tuning of SPL voxels with respect to maze-path direction. This finding is in accordance with the discovery of directional tuning to maze-path direction of single cells recorded in the posterior parietal cortex of monkeys performing a practically identical task (Crowe et al. 2004). Remarkably, the average tuning function of single voxels was very similar to that of single cells: in both cases, signal intensity dropped to 50–60% of its maximum at directions ±45° away from the preferred direction (Fig. 6). In addition, the prevalence of directional tuning in the population with a significant directional effect in the ANOVA was very similar in both cases, at ~50% [i.e., 51% in this study (see above) and 280/529 = 53% in the single-cell study (Crowe et al. 2004)]. It is noteworthy that this tuning was not because of passive visual or eye movement-related responses, as evidenced by the results of appropriate visuosensory and eye movement control tasks in the monkey (Crowe et al. 2004). It is also interesting that directional tuning was observed in both experiments even though the maze-path directions were randomized in the single-cell experiments but was blocked in the imaging experiments. The common property in both experiments is the mental traversing of the maze path, and this is the most likely explanation of the directional tuning.

The directional tuning of single voxels indicates that the associated BOLD intensity very probably reflects coherent, directionally selective synaptic activity of spatially close neuronal ensembles; on the other hand, the lack of tuning in a given voxel might suggest either a true absence of tuning or, alternatively, locations of transition in preferred directions, such that no coherent directionality is detected by the BOLD signal. Be that as it may, the direction of the maze path is obviously a major factor influencing neuronal activity in posterior parietal cortex, recorded directly electrophysiologically or reflected in the BOLD signal. This is in accord with the results of studies which demonstrated the detrimental effects of restricted lesions of the posterior parietal cortex on route-following in monkeys (Petrides and Iversen 1979).

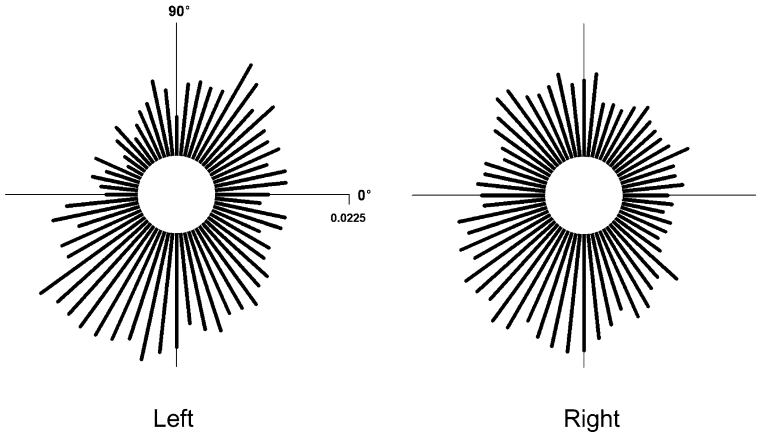

Fig. 7 Distribution of preferred directions in the two hemispheres in the form of circular histograms. Scale is relative frequency

The results of behavioral studies in human subjects and monkeys (Crowe et al. 2000a, b; Chafee et al. 2002) have suggested that the maze-solving task used in this study involves mental traversing of the maze path. This is a spatial–cognitive operation which is likely to involve various subprocesses, including spatial attention, object-based cognition, path integration, etc. Be that as it may, it is a time-consuming process and is analogous to the mental scanning of visual images (Kosslyn 1980). Indeed, this mental traversing of the maze path was visualized using the neuronal population vector (Crowe et al. 2000b) which pointed in the direction of the presumed mental traversing. Similarly, the neuronal population vector in the current study also pointed in the direction of the presumed mental traversing from the center outwards. As far as we are aware, this is the first time that the population vector has been successfully applied to fMRI data in general and to voxels in small locales in particular.

The congruence of neurophysiological and fMRI results with respect to both tuning and the population vector reinforces the close correspondence between electrophysiological and BOLD measures postulated on other grounds (Logothetis et al. 2002). In addition, the high signal-to-contrast ratio and higher spatial specificity afforded by the high magnetic fields (Ugurbil et al. 2003) further validates the accuracy of the localization of the effects, and hence the directional mapping observed. Finally, it is noteworthy that practically identical findings were obtained in preliminary studies using ultra-high magnetic field (7 T) (Tzagarakis et al. 2003).

Functional layout of SPL

The results of this study provide constraints for, and suggest a possible functional organization of, the SPL. The constraint comes from the finding that the average intercluster distance between a particular direction and all others was ~3 mm. This indicates that voxels with diverse preferred directions are close together, in a patch. This is also evidenced by the good prediction of the maze-path direction yielded by the population vector calculated within parts of the SPL. On the other hand, the average

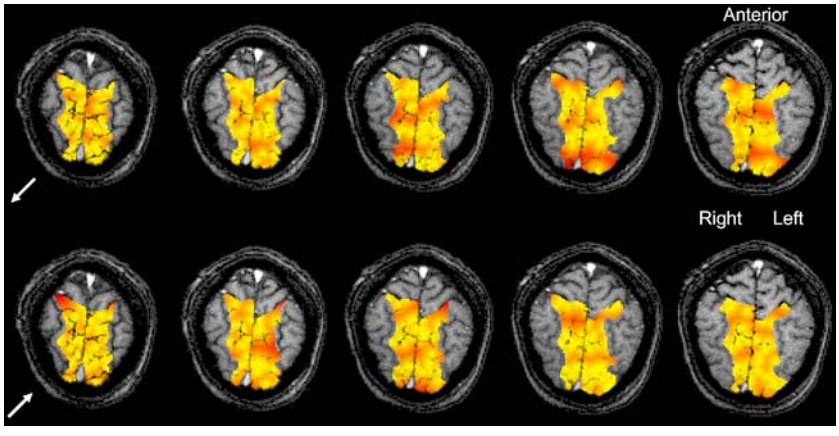

Fig. 8 Nearest neighbor plots for two opposite directions in all five slices of a single subject. For this analysis, preferred directions were binned to eight 45° intervals centered at 3 o'clock and every 45° thereafter. Given a specific voxel, the distance was calculated between this voxel and its nearest voxel with (binned) preferred direction in the direction of the *white arrow* (reference direction). *Colored areas* indicate the SPL; the color variation, from *light yellow* → *red*, corresponds to short → long distances, respectively. Therefore, *light yellow areas* indicate high concentration of voxels tuned to the reference direction, whereas *dark red areas* denote absence of voxels tuned to the reference direction

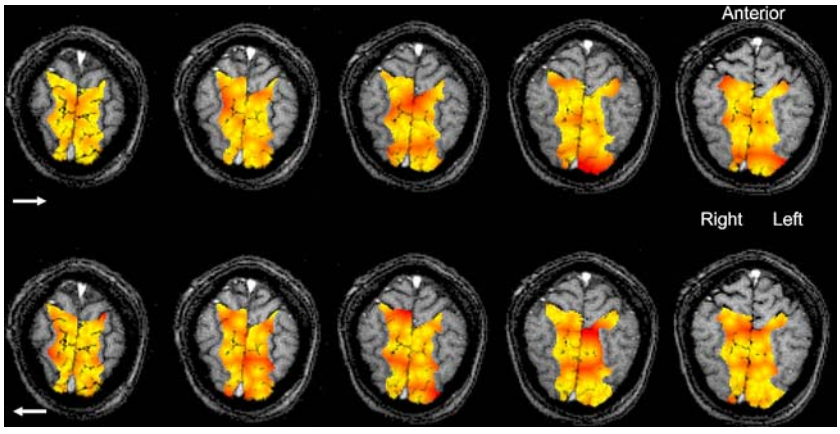

Fig. 9 Nearest-neighbor plots for two different opposite directions in all five slices of the same subject as in Fig. 8

same-direction nearest-neighbor intercluster distance was ~13 mm, which is actually an estimate of the average distance between nearest directional patches. Obviously, the remaining voxels, in the patches in-between, are not directionally tuned. Because 42% of all voxels were directionally tuned, the percentage of non-tuned voxels is 58%. Overall, then, these findings support the hypothesis of a patchy arrangement where patches of directionally tuned voxels, containing voxels with different preferred directions, alternate with patches of non-tuned voxels. Directional tuning in space has been a common func-

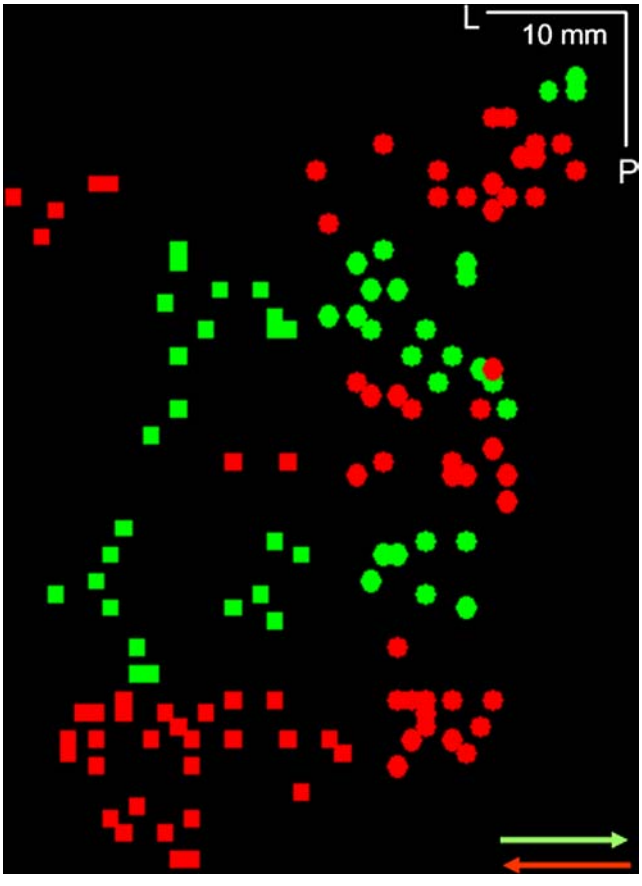

Fig. 10 Spatial distribution of directionally tuned voxels in a single slice. *Red* and *green* are preferred directions at 3 and 9 o'clock (±22.5°), respectively; *squares* and *circles* refer to left and right hemisphere, respectively

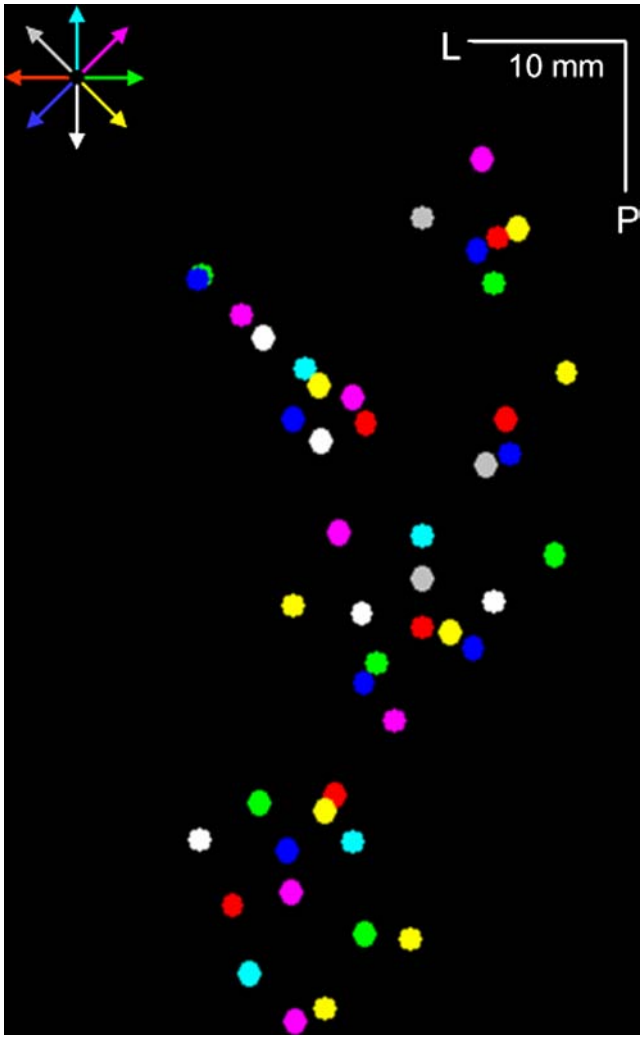

Fig. 11 Centers of clusters of preferred directions grouped in eight bins in a single slice of the left hemisphere. Color codes for the binned directions are indicated by the color wheel

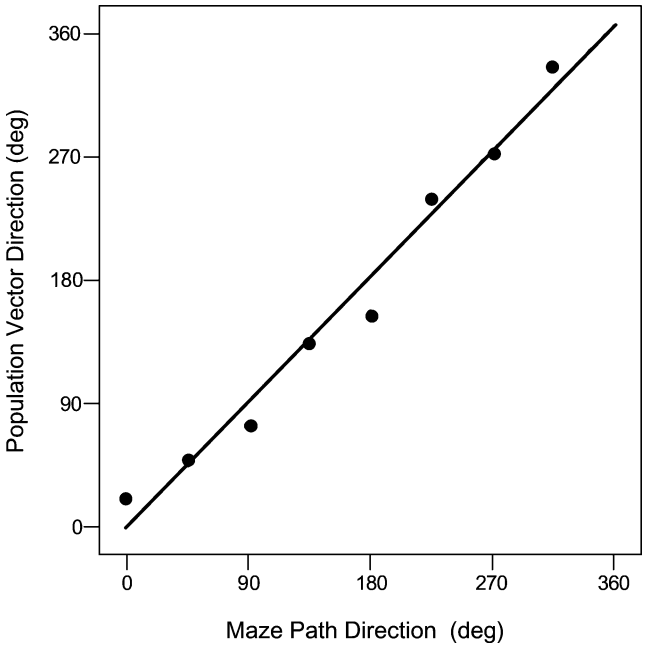

Fig. 12 The direction of the population vector computed from all the data is plotted against the corresponding direction of the maze path

tional property of neurons in the posterior parietal cortex of monkeys with respect to various visuomotor tasks (see Battaglia-Mayer et al. 2003, for a review), and dysfunction in this tuning has been proposed as a mechanism underlying optical ataxia (Battaglia-Mayer and Caminiti 2002). On the cognitive side, a consistent and strong involvement of SPL in mental rotation has been found in various studies (Cohen et al. 1996; Tagaris et al. 1996, 1997, 1998; Alivisatos and Petrides 1997; Harris et al. 2000, 2003; Bestmann et al. 2002) and well documented in

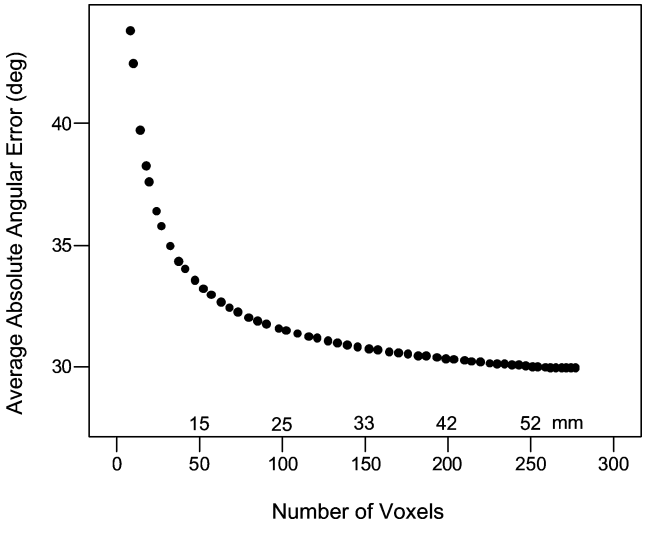

Fig. 13 The average absolute angular error of the population vector direction is plotted against the average number of voxels used in the calculation. The radius of space (in mm) from which the population vector was computed is also given above the abscissa

single-trial fMRI studies (Richter et al. 1997, 2000). Because mental tracing and mental rotation involve motion in imagined space, it would be interesting to know whether the directionally tuned voxels identified in this study would also show a significant activation in mental rotation, or, whether the latter process is carried out by the remainding (non-tuned) voxels. This remains to be investigated. Of course, several other areas are involved in maze solving/mental tracing, and the specific role of the SPL among them must be assessed quantitatively in a way, e.g., similar to that applied to mental rotation (Tagaris et al. 1996, 1998) and memory scanning (Tagaris et al. 1998).

Acknowledgements This work was supported by United States Public Health Service grant NS32919, NIH RR08079, the University of Minnesota Graduate School (TAJ), the MIND Institute, the KECK Foundation, the United States Department of Veterans Affairs, and the American Legion Chair in Brain Sciences. P.G. was supported by the Medical Corps Directorate of the Hellenic Army General Staff.

References

Aldenderfer MS, Blashfield RK (1984) Cluster analysis. Sage, Newbury Park CA

Alivisatos B, Petrides M (1997) Functional activation of the human brain during mental rotation. Neuropsychologia 35:111–118

Angelini R, Frasca R, Grossi D (1992) Are patients with constructional disorders different in visuo-spatial abilities? Acta Neurol 14:595–604

Battaglia-Mayer A, Caminiti R (2002) Optic ataxia as a result of the breakdown of the global tuning fields of parietal neurons. Brain 125:225–237

Battaglia-Mayer A, Caminiti R, Lacquaniti F, Zago M (2003) Multiple levels of representation of reaching in the parieto-frontal network. Cereb Cortex 13:1009–1022

Benton AL (1967) Constructional apraxia and the minor hemisphere. Confin Neurol 29:1–16

Bestmann S, Thilo KV, Sauner D, Siebner HR, Rothwell JC (2002) Parietal magnetic stimulation delays visuomotor mental rotation at increased processing demands. Neuroimage 17:1512–1520

Chafee MV, Averbeck BB, Crowe DA, Georgopoulos AP (2002) Impact of path parameters on maze solution time. Arch Ital Biol 140:247–251

Cohen MS, Kosslyn SM, Breiter HC, DiGirolamo GJ, Thompson WL, Anderson AK, Brookheimer SY, Rosen BR, Belliveau JW (1996) Changes in cortical activity during mental rotation. A mapping study using functional MRI. Brain 119:89–100

Corter JE (1996) Tree models of similarity and association. Sage, Newbury Park CA

Crowe DA, Averbeck BB, Chafee MV, Georgopoulos AP (2000a) Mental maze solving. J Cognitive Neurosci 12:813–827

Crowe DA, Chafee MV, Averbeck BB, Georgopoulos AP (2000b) Dynamic spatial processing of maze stimuli in area 7a. Soc Neurosci Abstr 26:2224

Crowe DA, Chafee MV, Averbeck BB, Georgopoulos AP (2004) Neural activity in primate parietal area 7a related to spatial analysis of visual mazes. Cereb Cortex 14:23–34

Georgopoulos AP, Kalaska JF, Caminiti R, Massey JT (1982) On the relations between the direction of two-dimensional arm movements and cell discharge in primate motor cortex. J Neurosci 2:1527–1537

Georgopoulos AP, Whang K, Georgopoulos MA, Tagaris GA, Amirikian B, Richter W, Kim S-G, Ugurbil K (2001) J Cognitive Neurosci 13:72–89

Harris IM, Miniussi C (2003) Parietal lobe contribution to mental rotation demonstrated with rTMS. J Cognitive Neurosci 15:315–323

Harris IM, Egan GF, Sonkkila C, Tochon-Danguy HJ, Paxinos G, Watson JD (2000) Selective right parietal lobe activation during mental rotation: a parametric PET study. Brain 123:65–73

Kosslyn SM (1980) Image and mind. Harvard University Press, Cambridge MA

Lewis SM, Jerde TA, Tzagarakis C, Tsekos N, Amirikian B, Georgopoulos MA, Kim S-G, Ugurbil K, Georgopoulos AP (2002) Logarithmic transformation for BOLD fMRI data. Soc Neurosci Abst 506.7

Lewis SM, Jerde TA, Tzagarakis C, Georgopoulos MA, Tsekos N, Amirikian B, Kim S-G, Ugurbil K, Georgopoulos AP (2003) Cerebellar activation during copying geometrical shapes. J Neurophysiol 90:3874–3887

Logothetis N, Merkle H, Augath M, Trinath T, Ugurbil K (2002) Ultra high-resolution fMRI in monkeys with implanted RF coils. Neuron 35:227–242

Marchini JL, Ripley BD (2000) A new statistical approach to detecting significant activation in functional MRI. Neuroimage 12:366–380

Mardia KV (1972) Statistics of directional data. Academic, New York NY

Petrides M, Iversen SD (1979) Restricted posterior parietal lesions in the rhesus monkey and performance on visuospatial tasks. Brain Res 161:63–77

Richter W, Ugurbil K, Georgopoulos AP, Kim S-G (1997) Time-resolved fMRI of mental rotation. Neuroreport 8:3697–3702

Richter W, Somorjai R, Summers R, Jarmasz M, Tegeler C, Ugurbil K, Menon R, Gati JS, Georgopoulos AP, Kim S-G (2000) Motor area activity during mental rotation studied by time-resolved single-trial fMRI. J Cognitive Neurosci 12:310–320

Snedecor GW, Cochran WG (1989) Statistical methods, 8th ed. Iowa State University Press, Ames IA

Tagaris GA, Kim S-G, Strupp JP, Andersen P, Ugurbil K, Georgopoulos AP (1996) Quantitative relations between parietal activation and performance in mental rotation. Neuroreport 7:773–776

Tagaris GA, Kim S-G, Strupp JP, Andersen P, Ugurbil K, Georgopoulos AP (1997) Mental rotation studied by functional magnetic resonance imaging at high field (4 Tesla): Performance and cortical activation. J Cognitive Neurosci 9:419–432

Tagaris GA, Richter W, Kim S-G, Pellizer G, Andersen P, Ugurbil K, Georgopoulos AP (1998) Functional magnetic resonance imaging of mental rotation and memory scanning: a multidimensional scaling analysis of brain activation patterns. Brain Res Rev 26:106–112

Tzagarakis C, van der Moortele P, Adriany G, Lewis SM, Gourtzelidis P, Humbert F, Ugurbil K, Georgopoulos AP (2003) Functional imaging of the superior parietal lobule (SPL) at ultra high magnetic field (7 Tesla) during performance of a maze task. Soc Neurosci Abst 182.2

Ugurbil K, Toth L, Kim D-S (2003) How accurate is magnetic resonance imaging of brain function? Trends Neurosci 26:108–114